Mathematical Problems in Engineering
Volume 3, pp. 267–286
Reprints available directly from the publisher
Photocopying permitted by license only

A 2D Finite Element Procedure for Magnetic Field Analysis taking into Account a Vector Preisach Model

LUC R. DUPRÉ[a,*], ROGER VAN KEER[b] and JAN A. A. MELKEBEEK[a]

[a]*Department of Electrical Power Engineering, University of Gent, Sint-Pietersnieuwstraat 41, B-9000 Gent, Belgium;* [b]*Department of Mathematical Analysis, University of Gent, Galglaan 2, B-9000 Gent, Belgium*

(Received 1 July 1996)

The main purpose of this paper is to incorporate a refined hysteresis model, viz. a vector Preisach model, in 2D magnetic field computations. To this end the governing Maxwell equations are rewritten in a suitable way, which allows to take into account the proper magnetic material parameters and, moreover, to pass to a variational formulation. The variational problem is solved numerically by a FE approximation, using a quadratic mesh, followed by the time discretisation based upon a modified Cranck Nicholson algorithm. The latter includes a suitable iteration procedure to deal with the nonlinear hysteresis behaviour. Finally, the effectiveness of the presented mathematical tool has been confirmed by several numerical experiments.

Keywords: Magnetic field analysis; vector hysteresis model; finite element-finite difference approximation; memory properties

Classification Categories: 35K55, 65M05, 65N30, 72A25

1 INTRODUCTION

In this paper we present the inclusion of the vector Preisach model, as described in [5], in the magnetic field calculations in a 2D-domain D. This

*Corresponding author. Tel.: +32 926 34 24. Fax: +32 9 264 35 82. E-mail: dupre@elmape.rug.ac.be.

domain D represents one tooth region of the stator of an asynchronous machine, as shown in Fig. 1.

In the conventional magnetic field analysis which is applied to rotating machines, the magnetic properties have been modeled by using a single valued material characteristic. Such kind of numerical modeling can not describe the material behaviour sufficiently accurate.

In [7] and [8] the magnetic behaviour of the material has been described in terms of the *unidirectional* macroscopic fields, using a scalar Preisach model to take into account the hysteresis phenomena.

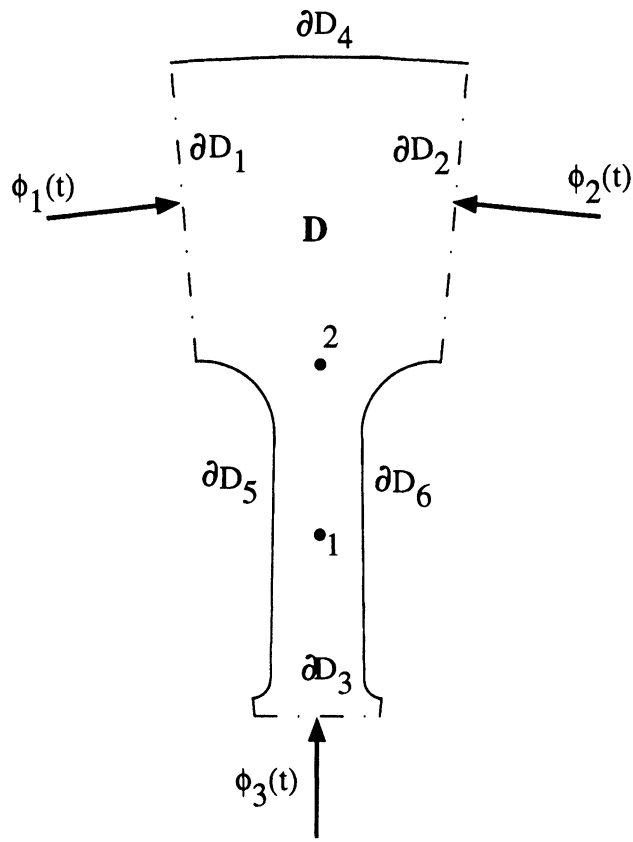

FIGURE 1 Model of one tooth region

In a *2D* domain, a *vector* hysteresis model is needed due to the local rotating magnetic flux excitations. These rotating flux excitations in electrical machines result from the complexity of the magnetic circuit and of the magnetic motoric force distributions.

An outline of the paper is now in order. In the next section we state the physical problem and its mathematical model. To be able to take properly into account the material characteristics in the vector Preisach model, the Maxwell equations must be rewritten in a nonstandard way. The variational formulation of the resulting boundary value problem for the scalar magnetic potential $\varphi(x, y, t)$ is derived in Section 3. This forms the basis for the fully discrete finite element—finite difference approximation method outlined in considerable detail in Section 4. Finally, we present in Section 5 a few numerical results for the local field patterns, which allow, for the magnetic analysis of rotating electrical machines, a comparison between the presented model and the more common models based on a single valued material characteristic. The discrepancies found in the local field patterns will have to be investigated further as with respect to their influence on the numerical results for the iron losses in electrical machines, which is a topic of ongoing research.

2 PHYSICAL PROBLEM AND MATHEMATICAL MODEL

2.1 Governing Equations in One Tooth Region D

The magnetic behaviour of the material can be described in terms of the macroscopic fields, taking into account the hysteresis phenomena.

We consider a single tooth region, see Fig. 1, where the electrical conductivity σ is assumed to be zero. The corresponding Maxwell equations for the magnetic field $\overline{H} = H_x\overline{1}_x + H_y\overline{1}_y$ and the magnetic induction $\overline{B} = B_x\overline{1}_x + B_y\overline{1}_y$, in the 2D domain D are, see e.g [4],

$$rot\overline{H} = 0 \tag{1}$$

$$div\overline{B} = 0 \tag{2}$$

where the relation between $\overline{H}$ and $\overline{B}$ is defined by the material characteristics obtained by the vector Preisach hysteresis model, described below. The boundary ∂D is divided into six parts ∂D_1, ∂D_2, ..., ∂D_6, see again Fig. 1. Enforcing a total flux $\phi_s(t)$ through the parts ∂D_s, s = 1, 2, 3, we arrive at the boundary conditions (BCs)

$$\phi_s(t) = \int_{\partial D_s} \overline{B} \cdot \overline{n} dl, \, t > 0, \, s = 1, 2, 3, \tag{3}$$

$$\overline{H} x \overline{n} = 0 \; on \; \partial D_s, \, t > 0, \, s = 1, 2, 3, \tag{4}$$

where $\overline{n}$ is the unit outward normal vector to the boundary part ∂D_s. At the other hand a zero flux leakage through ∂D_4, ∂D_5 and ∂D_6 results in the complementary BCs:

$$\overline{B} \cdot \overline{n} = 0 \; on \; \partial D_s, \, t > 0, \, s = 4, 5, 6. \tag{5}$$

The demagnetized state of the material at $t = 0$ is expressed by the initial condition (IC)

$$\overline{H}(x, y, t = 0) = 0, \, \forall (x, y) \in D. \tag{6}$$

2.2 Hysteresis Models

For an outline of the numerical model presented in this paper, we first briefly recall some basic principles of the vector Preisach model, as related to the more common scalar Preisach model. We may refer e.g. to [5],[6] and [9] respectively for the details.

2.2.1 Scalar Preisach Model

The *BH*-relation can be described by a scalar Preisach model if $\overline{H}$ and $\overline{B}$ are unidirectional.

In the Preisach model the material is assumed to consist of small dipoles, each being characterized by a rectangular hysteresis loop as shown in Fig. 2. The magnetisation of the dipole M_d takes the value -1 or $+1$, depending on the component $H(t)$ of the magnetic field and its history,

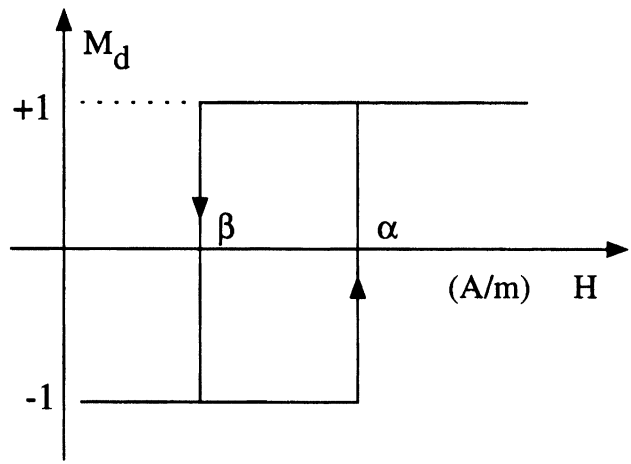

FIGURE 2 (M_d, H)-characteristic of a Preisach dipole

denoted by $H_{past}(t)$. The characteristic parameters α and β are distributed statistically according to a Preisach function $P_s(\alpha, \beta)$, which takes on a nonzero value in the triangle $\{(\alpha, \beta) | -H_m \leq \alpha \leq H_m, -H_m \leq \beta \leq \alpha\}$, see [9]. This distribution function $P_s(\alpha, \beta)$ is a material parameter, which can be identified directly using a well defined measurement technique, see e.g. [8] and [3]. The BH-relation (with $\overline{B} = B\overline{1}_x$) is given by

$$B(H, H_{past}) = \int_{-H_m}^{H_m} d\alpha \int_{-H_m}^{\alpha} d\beta \, \eta_s(\alpha, \beta, t) P_s(\alpha, \beta) \tag{7}$$

Here $\eta_s(\alpha, \beta, t)$ takes the time dependent value of the magnetisation M_d for the dipole with parameters α and β. Consequently the induction B depends upon $H(t)$ and $H_{past}(t)$.

2.2.2 Vector Preisach model

In the 2D domain D, the magnetic field $\overline{H}$ may rotate in the (x, y)-plane. Therefore we must pass to a vector hysteresis model.

In the vector Preisach model, as described in [5] and [6], the vector $\overline{H}$ is projected on an axis $\overline{d}$, which encloses an angle θ with the fixed x-axis, $-\pi / 2 < \theta < \pi / 2$, see Fig. 3. The corresponding value $H_d (= H_x cos\theta + H_y sin\theta)$ is taken to be the input of a scalar Preisach model on the axis $\overline{d}$.

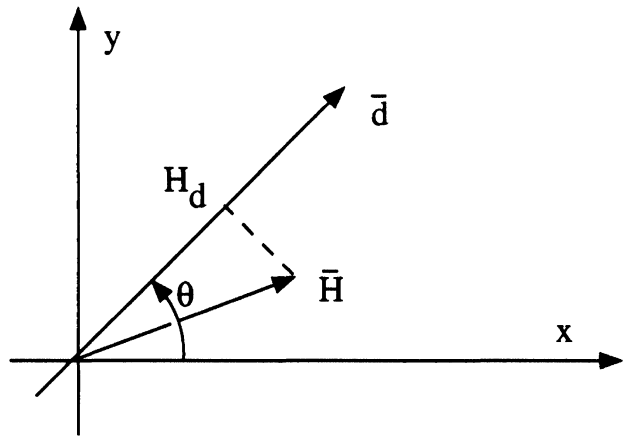

FIGURE 3 Vector Preisach model

The *BH*-relation is now given by, see [5],

$$\bar{B}(\bar{H}, \bar{H}_{past}) = \frac{1}{\pi} \int_{-\frac{\pi}{2}}^{\frac{\pi}{2}} \bar{1}_\theta d\theta \int_{-H_m}^{H_m} d\alpha \int_{-H_m}^{\alpha} d\beta \, \eta_r(\theta, \alpha, \beta, t) P_r(\theta, \alpha, \beta) \tag{8}$$

Notice that $\eta_r(\theta, \alpha, \beta, t)$ is obtained from the component $H_d(\theta, t)$, similarly as in the scalar Preisach model. Consequently $\bar{B}$ depends on $\bar{H}(t)$ and $\bar{H}_{past}(t)$. The dependency of P_r on θ reflects the anisotropy of the material.

3 TRANSFORMATION OF THE PROBLEM AND VARIATIONAL FORMULATION

First, we rewrite the Maxwell equations (1)–(2) in a suitable form. From (1) a scalar potential $\varphi(x, y, t)$ may be introduced such that $\bar{H} = -grad\varphi$ (of course, φ can only be determined apart from a constant, the choice of which will be specified below). Rewriting, in a classical way, the Maxwell equations in terms of this scalar potential doesn't allow to take into account in a proper way the material characteristics in the vector Preisach model. To overcome this difficulty, notice that the differential permeabilities $\mu_{xx} = \partial B_x/\partial H_x$, $\mu_{xy} = \partial B_x/\partial H_y$, $\mu_{yx} = \partial B_y/\partial H_x$ and $\mu_{yy} = \partial B_y/\partial H_y$ are *uniquely* defined by the vector Preisach model. Hence a suitable reformu-

lation of the problem should incorporate the material characteristics by means of these permeabilities. Therefore, we pass to the auxiliarly unknown u, defined as $u(x, y, t) = \dfrac{\partial \varphi}{\partial t}$.

Indeed, considering the time derivative of (2), we get

$$-\frac{\partial B_x}{\partial t} = \mu_{xx}\frac{\partial u}{\partial x} + \mu_{xy}\frac{\partial u}{\partial y}, \tag{9}$$

$$-\frac{\partial B_y}{\partial t} = \mu_{yx}\frac{\partial u}{\partial x} + \mu_{yy}\frac{\partial u}{\partial y}, \tag{10}$$

and consequently

$$\frac{\partial}{\partial x}\left(\mu_{xx}\frac{\partial u}{\partial x} + \mu_{xy}\frac{\partial u}{\partial y}\right) + \frac{\partial}{\partial y}\left(\mu_{yx}\frac{\partial u}{\partial x} + \mu_{yy}\frac{\partial u}{\partial y}\right) = 0. \tag{11}$$

The boundary conditions (3)-(4)-(5) lead to

$$\frac{d\phi_s(t)}{dt} = \int_{\delta D_s} \frac{d\bar{B}}{dt} \cdot \bar{n} dl, t > 0, s = 1, 2, 3 \tag{12}$$

$$\varphi = C_s(t) \text{ on } \partial D_s, t > 0, s = 1, 2, 3 \tag{13}$$

and

$$\frac{d\bar{B}}{dt} \cdot \bar{n} = 0 \text{ on } \partial D_s, t > 0, s = 4, 5, 6. \tag{14}$$

Here, to remove the degree of freedom involved in the scalar potential φ, we *choose*

$$\varphi = 0 \text{ on } \partial D_3, t > 0. \tag{15}$$

We must add the IC resulting from (6) and (15), viz.

$$\varphi = 0, \forall (x, y) \in D, t = 0. \tag{16}$$

Source conditions.
Two types of source conditions occur.

(a) With ϕ-*type excitation*, the total flux $\phi_s(t)$ through ∂D_s, s = 1, 2, 3 is enforced (of course with $\Sigma_{s=1}^{3} \phi_s(t) = 0, t > 0$). Then, the uniform but time depending value of the scalar potential φ on ∂D_s, denoted by $C_s(t)$, $s = 1$ or 2, is not given a priori, but must be determined as part of the problem.
(b) With so called φ-*excitation* the uniform value $\varphi(t) = C_s(t)$, $t > 0$, at ∂D_s, $s = 1$ and 2, is enforced, (recall (15)). From the boundary value problem (11), (13)–(14), (16), we may obtain the magnetic induction $\overline{B}$. Then the total flux $\phi_s(t)$, $s = 1$, 2 or 3, follows from (12) and (16).

To derive a suitable variational form of this problem, we introduce the function space

$$V = \{v \in W_2^1(D);\ v|_{\partial D_s} \text{ is a constant depending on s, } s = 1, 2, 3\} \tag{17}$$

Here $W_2^1(D)$ is the usual first order Sobolov space on D and the condition "$v|_{\partial D_s}$ is constant" must be understood in the sense of traces, as defined e.g. in [1]. Then multiplying both sides of (11) with a test function $v(x, y) \in V$, integrating over D, applying Green's theorem and invoking the boundary condition (12), the problem (11)–(16) is found to be (formally) equivalent with the following variational problem:

Find a function $\varphi(x, y, t)$ *with* $u(x, y; t) = \dfrac{\partial \varphi}{\partial t}$,
obeying $\varphi \in V$ *and* $\dfrac{\partial \varphi}{\partial t} \in L_2(D)$ *for every* $t > 0$, *such that*

$$\int_D (\mu_{xx} \frac{\partial u}{\partial x} + \mu_{xy} \frac{\partial u}{\partial y}) \frac{\partial v}{\partial x} + (\mu_{yx} \frac{\partial u}{\partial x} + \mu_{yy} \frac{\partial u}{\partial y}) \frac{\partial v}{\partial y}\, dxdy = \sum_{s=1}^{3} \frac{d\phi_s(t)}{dt} v|_{\partial D_s} \tag{18}$$

$$\text{for every } v \in V,\ t > 0$$

and

$$\varphi = 0, \text{ for t} = 0. \tag{19}$$

Notice that by the requirement $\varphi \in V$ for every $t > 0$, (13) is automatically taken into account.

4 FINITE ELEMENT-FINITE DIFFERENCE APPROXIMATION

4.1 Space Discretisation by Finite Elements

For a usual triangulation τ_h of the domain D, (h mesh parameter), shown in Fig. 4, we consider a quadratic finite element mesh.

By $N_j(x, y)$, $(j = 1,\ldots, J)$, we denote the *standard cardinal* basis functions, associated to the nodes (x_j, y_j), $(j = 1,\ldots, J)$, J being the total number of nodes. Here, the nodes are numbered such that the first I of them, $I < J$, belong to the domain D or to the boundaries ∂D_4, ∂D_5 and ∂D_6. On the boundaries ∂D_1, ∂D_2 and ∂D_3 we have J_1, J_2 and J_3 nodes respectively, $(J - I = J_1 + J_2 + J_3)$. We then have, with $C^0(\overline{D})$ being the space of continuous functions on $\overline{D}$ and with $P_2(T)$ being the space of polynomials of degree ≤ 2 on T, see e.g. [1],

$$X_h \equiv \{v \in C^0(\overline{D}) \; |v|_T \in P_2(T), \forall T \in \tau_h\} = span(N_j)_{j=1}^{J} \tag{20}$$

and

$$X_{0h} \equiv \{v \in X_h \mid v = 0 \; on \; \partial D_s, \; s = 1, 2, 3\} = span(N_j)_{j=1}^{I} \tag{21}$$

Next we introduce

$$\psi_{I+1}(x, y) = \sum_{j=I+1}^{I+J_1} N_j(x, y), \tag{22}$$

$$\psi_{I+2(x,y)} = \sum_{j=I+J_1+1}^{I+J_1+J_2} N_j(x, y), \tag{23}$$

$$\psi_{I+3}(x, y) = \sum_{j=I+J_1+J_2+1}^{J} N_j(x, y) \tag{24}$$

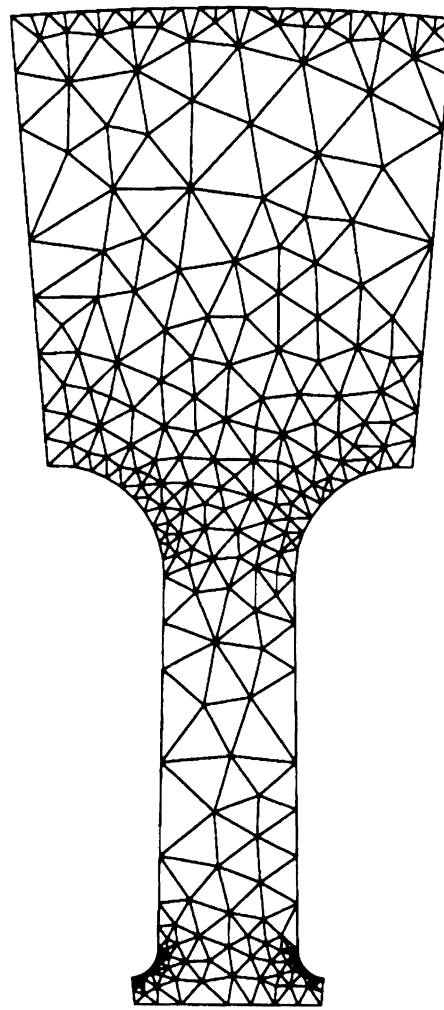

FIGURE 4 Triangulation τ_h for the domain D

Evidently, ψ_{I+1}, ψ_{I+2} and ψ_{I+3} belong to the space X_h. On a side ζ of the triangle $T \in \tau_h$, for which $\zeta \subset \partial D_s$, we have $\psi_{I+s}|_\zeta \equiv 1$, as clearly $\psi_{I+s}|_\zeta$ is a quadratic function of one local variable showing the value 1 in the 3 nodes on ζ. Consequently:

$$\psi_{I+s} \equiv 1 \text{ on } \partial D_s,\ s = 1, 2, 3. \tag{25}$$

Moreover ψ_{I+s} is readily understood to vanish throughout D apart from the triangles $T \in \tau_h$ adjacent to ∂D_s. Writing, for convenience, $\psi_j = N_j$, $1 \leq j \leq I$, we finally define:

$$V_h = span\,(\psi_j)_{j=1}^{I+3} = X_{0h} \oplus span\,(\psi_{I+s})_{s=1}^{3} \tag{26}$$

This space V_h is suitable for a conforming finite element approximation as $V_h \subset V$. Indeed, for $v \in V_h$ one evidently has $v \in X_h \subset W_2^1(D)$, while moreover v is constant on ∂D_1, ∂D_2 and ∂D_3, due to (25).

The finite element approximation $\varphi_h(x, y; t) \in V_h$ of $\varphi(x, y; t)$ is defined by a system similar to (18)–(19), now with V replaced by V_h. Here, we approximate the space dependency of μ_{kl}, by passing to $\hat{\mu}_{kl} \simeq \mu_{kl}$, defined by

$$\begin{aligned} &\hat{\mu}_{kl}(x, y, t, \varphi_h(x, y; t), \varphi_h^{(past)}(x, y; t)) = \\ &\mu_{kl}(x_T^c, y_T^c, t, \varphi_h(x_T^c, y_T^c, t), \varphi_h^{(past)}(x_T^c, y_T^c, t)) \\ &(x, y) \in T, \forall T \in \tau_h, t > 0 \end{aligned} \tag{27}$$

where (x_T^c, y_T^c) is the center of gravity of T. This allows us to take properly into account the nonlinear and hysteresis effects, resulting in the complicated form of the differential permeability μ_{kl}. Here, μ_{kl} now depends upon the finite element approximation $H_h(x,y;t) = -grad\varphi_h$ and $H_h^{(past)}(x, y; t) = -grad\varphi_h^{(past)}$ of the magnetic field $H(x, y; t)$ and its history $H^{(past)}(x, y; t)$, respectively.

Explicitly, recalling (15) and decomposing φ_h as

$$\varphi_h(x, y; t) = \sum_{j=1}^{I+2} \varphi_j(t)\psi_j(x, y), t > 0, \tag{28}$$

we have $\varphi_j(t) = \varphi_h(x_j, y_j; t)$, $1 \leq j \leq I$, and moreover $\varphi_{I+s}(t) = \varphi_h(x, y; t)|_{\partial D_s}$, $s = 1, 2$, due to the proper choice of the basis functions of V_h, (26).

Notice that in the case of ϕ-excitation (case (a) in Section 3), all coefficient functions $\varphi_j(t)$, $1 \leq j \leq I + 2$, are unknown, while in the case of φ-excitation (case (b) in Section 3), the coefficient function $\varphi_{I+1}(t)$ and $\varphi_{I+2}(t)$ are given.

These unknown coefficient functions will be derived from a system of first order ODEs, resulting from the finite element *discretisation* of (18). More precisely, take as test functions in (18) either $v = \psi_i(t)$, $1 \leq i \leq I + 2$ (case (a)), or $v = \psi_i(t)$, $1 \leq i \leq I$, (case (b)).

Thus, we are led to the following system

$$M(t, C(t), C^{(past)}(t)) \cdot \frac{dC}{dt} = F, t > 0 \tag{29}$$

along with the ICs, cf. (16),

$$C(0) = 0 \tag{30}$$

and

$$\begin{cases} \eta_r(x, y, \alpha, \beta, t = 0) = +1 : \alpha + \beta < 0 \\ \eta_r(x, y, \alpha, \beta, t = 0) = -1 : \alpha + \beta > 0 \end{cases}, \forall (x, y) \in D \tag{31}$$

The second IC corresponds to the history of the material at t = 0 (i.e. the demagnetized state of the material). Here, the matrices involved read as follows.

case (a)

C and $C^{(past)}$ are the column matrices,

$$C(t) = [\varphi_1(t), \varphi_2(t), \ldots, \varphi_{I+2}(t)]^T \tag{32}$$

$$C^{(past)}(t) = [\varphi_1^{(past)}(t), \varphi_2^{(past)}(t), \ldots, \varphi_{I+2}^{(past)}(t)]^T$$

while M is the mass matrix given by

$$M(t, C(t), C^{(past)}(t)) = (M_{l,m})_{1 \leq l,m \leq I+2}, \tag{33}$$

with

$$M_{l,m} = \int_D \left(\hat{\mu}_{xx} \frac{\partial \psi_l}{\partial x} \frac{\partial \psi_m}{\partial x} + \hat{\mu}_{xy} \frac{\partial \psi_l}{\partial x} \frac{\partial \psi_m}{\partial y} + \hat{\mu}_{yx} \frac{\partial \psi_l}{\partial y} \frac{\partial \psi_m}{\partial x} + \hat{\mu}_{yy} \frac{\partial \psi_l}{\partial y} \frac{\partial \psi_m}{\partial y} \right) dxdy \tag{34}$$

and finally the $(I + 2)$x1-force matrix F, corresponding to the RHS of (18), reads

$$F(t) = \frac{d\phi_1}{dt} \cdot [0, 0, \ldots, 0, 1, 0]^T + \frac{d\phi_2}{dt} \cdot [0, 0, \ldots, 0, 0, 1]^T \qquad (35)$$

where we used (25) and the fact that $\psi_1, \psi_2, \ldots, \psi_I$ all vanish on ∂D_1 and ∂D_2.

case (b)

C, $C^{(past)}$ and M take a similar form as in case (a), of course with the proper dimensions.

However the force matrix now has the form

$$F(t) = [F_1(t), F_2(t), \ldots, F_I(t)]^T \qquad (36)$$

with

$$F_i(t) = -M_{i,I+1} \frac{d}{dt} \varphi_{I+1}(t) - M_{i,I+2} \frac{d}{dt} \varphi_{I+2}(t), \; 1 \leq i \leq I \qquad (37)$$

4.2 Time Discretisation by Finite Differences

The IVP (29)–(31) is solved numerically by a suitable finite difference approximation method. We may restrict ourselves to the case of ϕ-excitation, (case (a)), the case of φ-excitation being completely analogous. The analysis proceeds similarly as in [2].

Let Δt be a time step and $t_k = k \cdot \Delta t$, $(k = 0, 1, 2, \ldots)$, be the corresponding equidistant time points. We define an approximation $C^{(k)} = [\varphi_1^{(k)}, \varphi_2^{(k)}, \ldots, \varphi_{I+2}^{(k)}]^T$ of $C(t_k) = [\varphi_1(t_k), \varphi_2(t_k), \ldots, \varphi_{I+2}(t_k)]^T$, $(k = 1, 2, \ldots)$, by the following recurrent algebraic system

$$\tilde{M}^{(k)} \cdot \frac{C^{(k)} - C^{(k-1)}}{\Delta t} = \frac{F(t_k) + F(t_{k-1})}{2}, \; k = 1, 2, \ldots \qquad (38)$$

starting from, see (30),

$$C^{(0)} = 0. \tag{39}$$

By means of $C^{(k)}$ we construct an approximation $\varphi_h^{(k)(x,y)}$ of $\varphi_h(x, y, t_k)$, (28), viz.

$$\varphi_h^{(k)}(x, y) = \sum_{j=1}^{I+2} \varphi_j^{(k)} \psi_j(x, y). \tag{40}$$

As the matrix $\tilde{M}^{(k)}$ depends on the unknown $C^{(k)}$, we set up an iterative procedure to solve the *nonlinear* system (38) at every time point t_k, the number of iterations being denoted by n_k. The approximation of $C^{(k)}$ at the l-th iteration level is denoted by $C^{(k),(l)}$. The corresponding approximation of (40) is written as $\varphi_h^{(k),(l)}(x, y)$. In the final iteration level we write $\varphi_h^{(k)} := \varphi_h^{(k),(n_k)}$, which is then used as the input at the subsequent time point t_{k+1}.

In the iterative procedure the matrix $\tilde{M}^{(k)}$, appearing in (38), is generated from the matrix M by a suitable averaging procedure over the interval $[t_{k-1}, t_k]$, as described in detail in [2]

5 NUMERICAL RESULTS

The effectiveness of the variational approximation for the problem (11)–(16) as outlined in the previous sections, has been confirmed by several numerical experiments, both for the case of ϕ-excitation and for the case of φ-excitation.

We considered a test problem with practical relevance, viz. the evaluation of the local fieldpatterns in one tooth region of an asynchronuous machine, shown in Fig. 1.

The numerical results obtained with the present model are compared with these resulting from more common models based upon one single valued material characteristic. More precisely, we will compare the numerical results for the time variation of $\overline{H}$ and $\overline{B}$ in selected points of the tooth region D. As both the scalar potential excitation and the flux excitation are periodic in time, we may use a complex Fourier decomposition for the local vector fields $\overline{H}(x, y; t)$ and $\overline{B}(x, y; t)$, viz.

$$\overline{H}(x, y; t) \equiv \sum_{k=-\infty}^{+\infty} H_k(x, y) \cdot e^{j(k\omega t + \alpha_k)} \tag{41}$$

$$\overline{B}(x, y; t) \equiv \sum_{k=-\infty}^{+\infty} B_k(x, y) \cdot e^{j(k\omega t + \beta_k)} \tag{42}$$

Here, ω is 2π times the basic frequency, α_k [resp. β_k] and H_k [resp. B_k] are the phase angle and the amplitude of the k-th harmonic of $\overline{H}$ [resp. $\overline{B}$]. For the magnetic material we used the Preisach function P_r such that

$$\int_{H_1}^{H_2} d\alpha \int_{H_1}^{\alpha} d\beta P_r(\alpha, \beta) = 13.10^{-6}|H_1 \quad - H_2| + 0.56\,(f(H_1) - f(H_2))(f(-H_2) - f(-H_1))$$
$$-H_m \leq H_1 \leq H_2 \leq H_m \tag{43}$$

with

$$f(x) = arctan(x/200) \tag{44}$$

We present numerical results for the 2 types of excitation mentioned above.

case1: φ-excitation

We enforce a simple time variation of the scalar potential at the boundary parts ∂D_1 and ∂D_2, viz.

$$\varphi_{I+1}(t) = \varphi_{max} cos(2\pi ft + \gamma_1) \tag{45}$$

and

$$\varphi_{I+2}(t) = -\varphi_{max} cos(2\pi ft + \gamma_2) \tag{46}$$

with $\varphi_{max} = 120, f = 50Hz, \gamma_1 = 25^o$ and $\gamma_2 = 6^o$. For this excitation we compute the field pattern in the domain D and we consider point 2 in Fig. 1. Fig. 5 reveals the difference between the B_xB_y-loci obtained with the vector Preisach model and the one obtained with the more common single valued material characteristic.

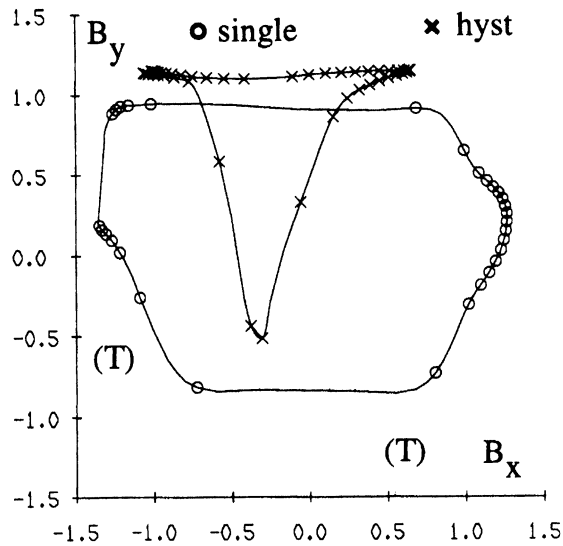

FIGURE 5 B_xB_y-loci in point 2, case 1

case2: ϕ-excitation

The enforced realistic fluxpatterns through ∂D_1 and ∂D_2 are

$$\phi_j(t) = a_{j,1}cos(2\pi ft + \gamma_{j,1}) + a_{j,15}cos(30\pi ft + \gamma_{j,15}) + a_{j,17}cos(34\pi ft + \gamma_{j,17}), j = 1, 2 \quad (47)$$

where the amplitudes and fase angles are given in Table I, and where $f = 50Hz$. We consider the 2 points indicated in Fig. 1, for which we expect a different type of field pattern. The corresponding B_xH_x-loop and B_yH_y-loops are shown in Fig. 6. Fig. 7 shows the *scaled* spectra of the amplitudes for the vectors $\overline{B}$ and $\overline{H}$ for point *1*, according to (41)-(42). Again the values obtained with the vector Preisach model deviates from those obtained with the single valued material characteristics (the more when the

TABLE I Amplitudes and angles of excitation in case 2

	Amplitudes (T)			*Fases (degree)*		
	1	15	17	1	15	17
ϕ_1	1.262	0.0178	0.0105	25.	109.	−36.
ϕ_2	1.268	0.0067	0.005	5.9	−155.	27.

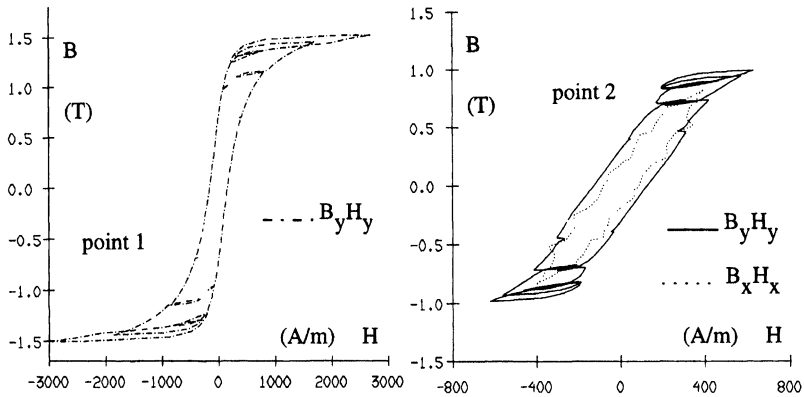

FIGURE 6 B_xH_x- and B_yH_y-loops in point 1 and point 2, case 2

scaling factors are different, as indicated). Moreover, notice the symmetry for each pair of positive and negative harmonics. This corresponds with alternating field vectors, which is in agreement with a qualitative property for points such as point *1* in *D*. This symmetry is lost in the case of point *2* in *D*, see Fig. 8, corresponding to rotational fields $\overline{H}$ and $\overline{B}$ in this point. For the sake of completeness, in Fig. 9 and Fig. 10 we show the phase angles α_k and β_k for the same points *1* and *2*. Again the difference between the results obtained with the vector Preisach model and those obtained with the single valued material characteristic are non neglectible.

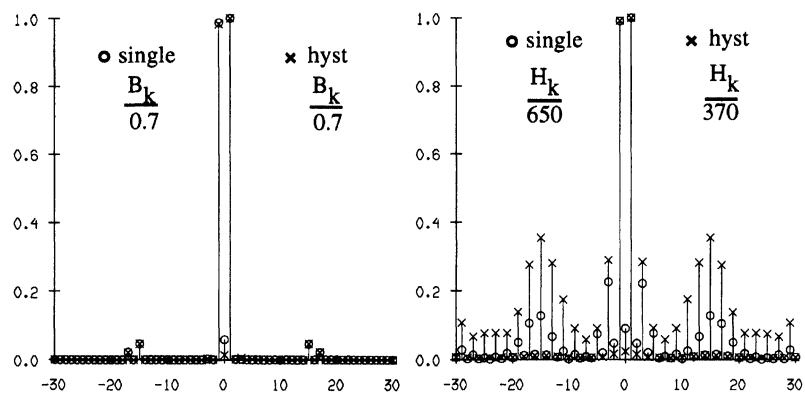

FIGURE 7 Spectrum of the amplitude of $\overline{B}$ and $\overline{H}$ in point 1, case 2

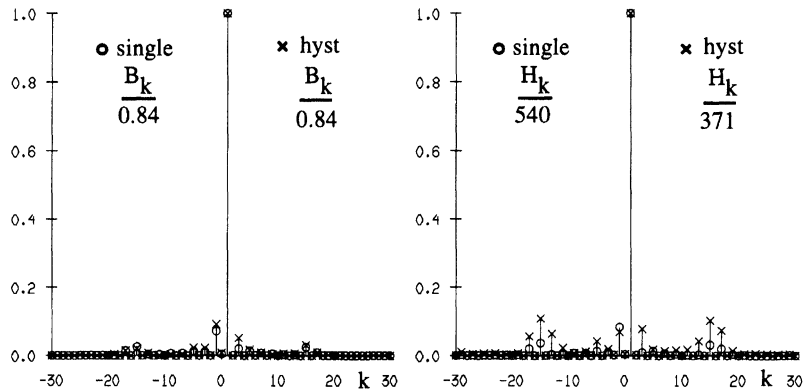

FIGURE 8 Spectrum of the amplitude of $\overline{B}$ and $\overline{H}$ in point 2, case 2

6 CONCLUSIONS AND FUTURE DIRECTIONS

In this paper we outlined a suitable numerical method for the evaluation of local field patterns in a 2D region, based upon a proper reformulation of the governing Maxwell equations. This allowed us to incorporate a refined hysteresis model, viz. a vector Preisach model, in the magnetic field computations. We found differences for the local field patterns when evaluated first with the vector Preisach model and next with the more common

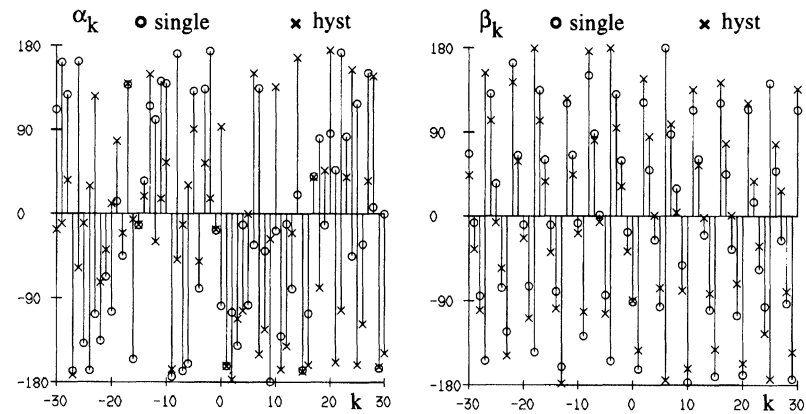

FIGURE 9 Spectrum of the angle of $\overline{B}$ and $\overline{H}$ in point 1, case 2

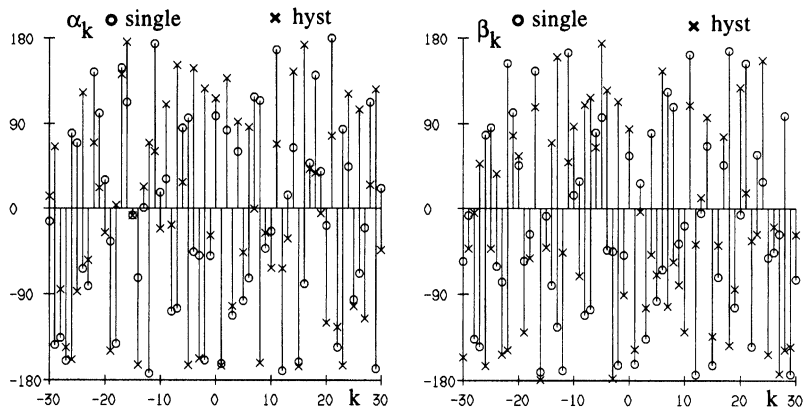

FIGURE 10 Spectrum of the angle of $\overline{B}$ and $\overline{H}$ in point 2, case 2

single valued material characteristic. It's a topic of further research to investigate the possible influence of these discrepancies on the numerical evaluation of the iron losses in rotating electrical machines.

Acknowledgment

We gratefully acknowledge the financial support by the Belgian Government in the frame of the Inter-University Attraction Poles for fundamental research.

References

[1] Ciarlet, P. G. (1978). *The Finite Element Method of Elliptic Problems*, North-Holland, Amsterdam.

[2] Dupré, L., Van Keer, R. and Melkebeek, J. (1996). On a Numerical model for the Evaluation of Electromagnetic Losses in Electric Machinery, *Int. J. of Num. Meth. in Eng.*, **39**, 1535–1553.

[3] Dupré, L., Van Keer, R. and Melkebeek, J. Modelling and identification of the iron losses in non-oriented steel laminations using the Preisach theory, *IEE Proc.—Elec. Power Appl.* (submitted).

[4] Halliday and Resnick. (1981). *Fundamental of Physics*, John Wiley & Sons, New York.

[5] Mayergoyz, I. D. (1991). *Mathematical models of hysteresis*, Springer Verlag, New York.

[6] Mayergoyz, I. D. and Friedman, G. (1987). Isotropic vector Preisach model of hysteresis, *J. Appl. Phys.*, **61**, 4022–4024.

[7] Philips, D., Dupré, L. Cnops, J. and Melkebeek, J. (1994). The Application of the Preisach Model in Magnetodynamics: Theoretical and Practical Aspects, *J. Magn. Magn. Mater.*, **133**, 540–543.
[8] Philips, D., Dupré L. and Melkebeek, J. (1994). Magneto-dynamic field computation using a rate-dependent Preisach model, *IEEE Trans. Mag.*, **30**, 4377–4379.
[9] Preisach, F. (1935). Uber the magnetische nachwirkung, *Zeits. füur Phys.*, **94**, 277–302.